LETTER

doi:10.1038/nature11940

Multiple phases of chondrocyte enlargement underlie differences in skeletal proportions

Kimberly L. Cooper[1]*, Seungeun Oh[2]*, Yongjin Sung[3], Ramachandra R. Dasari[3], Marc W. Kirschner[2] & Clifford J. Tabin[1]

The wide diversity of skeletal proportions in mammals is evident upon a survey of any natural history museum's collections and allows us to distinguish between species even when reduced to their calcified components. Similarly, each individual is comprised of a variety of bones of differing lengths. The largest contribution to the lengthening of a skeletal element, and to the differential elongation of elements, comes from a dramatic increase in the volume of hypertrophic chondrocytes in the growth plate as they undergo terminal differentiation[1–7]. However, the mechanisms of chondrocyte volume enlargement have remained a mystery[8–11]. Here we use quantitative phase microscopy[12] to show that mammalian chondrocytes undergo three distinct phases of volume increase, including a phase of massive cell swelling in which the cellular dry mass is significantly diluted. In light of the tight fluid regulatory mechanisms known to control volume in many cell types[13], this is a remarkable mechanism for increasing cell size and regulating growth rate. It is, however, the duration of the final phase of volume enlargement by proportional dry mass increase at low density that varies most between rapidly and slowly elongating growth plates. Moreover, we find that this third phase is locally regulated through a mechanism dependent on insulin-like growth factor. This study provides a framework for understanding how skeletal size is regulated and for exploring how cells sense, modify and establish a volume set point.

Each of the long bones initially forms in the embryo as a similarly sized cartilage rudiment that only subsequently undergoes differential regulation of growth. The elongation of a skeletal element occurs at the growth plate[14,15], each consisting of three distinct zones: resting round chondrocytes near the end of an element give rise to clonal columns of flattened proliferating chondrocytes that then terminally differentiate into hypertrophic chondrocytes nearest the bony centre of an element. Although multiple cellular parameters contribute to lengthening of skeletal elements—including proliferation, matrix deposition and hypertrophic cell enlargement—the greatest contribution to growth rate in mammals is due to the massive volume enlargement of hypertrophic chondrocytes expanding the skeletal tissue in the direction of longitudinal growth within laterally restricting matrix channels[1–3]. In addition to being the largest contributor to the elongation rate of a given skeletal element, this parameter is largely responsible for the difference in growth rates between different skeletal elements within an individual, between homologous elements in different species, and within a single element as an animal ages[4–7]. Surprisingly, however, given its critical importance in determining the growth rate of each bone and the overall stature of the individual, the mechanism is poorly understood. It even remains unclear whether hypertrophic chondrocyte volume increases by true hypertrophy, maintaining constant density during growth through an increase in macromolecules and organelles, or by cell swelling through disproportionate fluid uptake, which is ordinarily a hallmark of disease[13].

To determine whether hypertrophic chondrocytes enlarge by cellular hypertrophy and/or swelling, we applied methods of diffraction phase microscopy to measure the dry mass of individual unstained live cells dissociated from growth plate cartilage. (Fig. 1a and Supplementary Methods)[16]. Together with volume information about the sample, calculated here based on a well-supported spherical approximation for dissociated chondrocytes (Supplementary Methods), this allows the calculation of dry mass density. Diffraction phase microscopy measurements of a variety of cell types consistently reflect a 'normal' dry mass density for healthy living cells at approximately 0.182 pg per femtolitre (fl) in agreement with the concentration of cytoplasm previously determined by index matching in human oral epithelial cells[17].

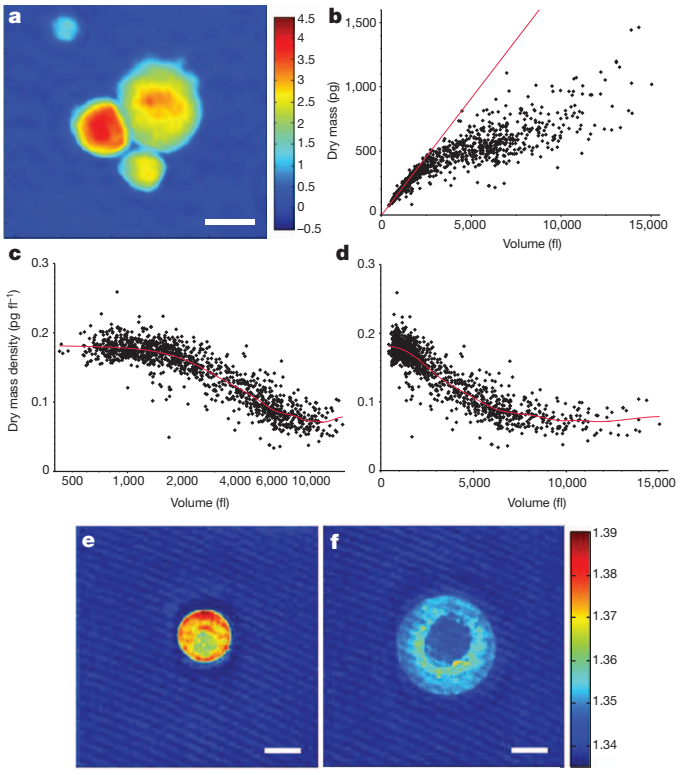

Figure 1 | Hypertrophic chondrocytes increase in volume through three distinct phases including a phase of massive cell swelling. **a**, Quantitative phase image of dissociated mouse proximal tibia hypertrophic chondrocytes at postnatal day 5 (P5). Colour bar represents phase shift in radians. **b**, Volume versus dry mass plotted for individual chondrocytes. Linear regression for cells up to 1,000 fl highlights divergence of larger cells from an initial slope of 0.183 pg fl^{-1}. **c**, **d**, Log scale (**c**) and linear scale (**d**) plots of volume versus dry mass density. Lambda for the smoothened spline in (**c**) and (**d**) is 5×10^9. R^2 value is 0.84. $n = 1{,}249$ cells summed across five independent experiments. **e**, **f**, Horizontal cross sections from regularized tomographic phase microscopy density reconstructions of a small (**e**) and large (**f**) mouse tibia chondrocyte. Colour bar represents refractive index and thus dry mass density. Scale bars, 10 μm.

[1]Department of Genetics, Harvard Medical School, Boston, Massachusetts 02115, USA. [2]Department of Systems Biology, Harvard Medical School, Boston, Massachusetts 02115, USA. [3]George R. Harrison Spectroscopy Laboratory, Massachusetts Institute of Technology, Cambridge, Massachusetts 02139, USA.
*These authors contributed equally to this work.

This includes maturing megakaryocytes that reach volumes comparable to the largest hypertrophic chondrocytes and ten times the average somatic cell volume (Supplementary Fig. 1).

In contrast, analysis of chondrocytes from the rapidly elongating mouse proximal tibia reveals that there are three distinct phases of hypertrophic cell enlargement. In phase 1, an initial increase of about threefold from approximately 600 fl to 2,000 fl is characterized by true hypertrophy—a proportionate increase in dry mass production and fluid uptake thus maintaining the normal dry mass density at 0.183 pg fl^{-1} (Fig. 1b, c). In phase 2, a fourfold enlargement from about 2,000 fl to 8,000 fl is characterized by cell swelling. Volume increases at a rate disproportionate to the continuing rate of dry mass production resulting in a dramatic dilution of dry mass density to approximately 0.07 pg fl^{-1} (Fig. 1c). In phase 3, at volumes larger than 8,000 fl, the dry mass density once again stabilizes, and cells continue to enlarge another twofold to about 14,000 fl by proportionately increasing dry mass and fluid volume at this lower density (Fig. 1d). Swelling in phase 2 allows cells to reach volumes two to three times greater in phase 3 than if they relied entirely on the proportionate increase in dry mass at high density (Fig. 1b, linear regression).

To verify that this decrease in density is characteristic of hypertrophic differentiation, we imaged a subset of the small high-density cells and large low-density cells using regularized tomographic phase microscopy to generate a refractive index map of dry mass density in three-dimensions (Supplementary Methods). This independent approach confirms that the largest cells reduce their dry mass density by approximately 60%, and moreover indicates that dry mass is low throughout the cytoplasm with a slightly higher density ring around the nucleus (Fig. 1e, f and Supplementary Fig. 14).

Understanding the cellular process by which hypertrophic cells enlarge provides a framework for considering how that process is modulated to achieve differential growth of individual elements within a species and of homologous elements between species. In contrast to the large hypertrophic chondrocytes of the rapidly elongating proximal tibia, the slowly elongating proximal radius has much smaller hypertrophic chondrocytes[1]. We find that these cells go through phase 1 and enter phase 2, similar to the cells of the proximal tibia, reaching a volume of approximately 5,000 fl. However, they truncate the remainder of phase 2 after dilution of dry mass density to approximately 0.10 pg fl^{-1} and completely eliminate phase 3 (Fig. 2a).

We next compared growth plates of the mouse to those of the lesser Egyptian jerboa, *Jaculus jaculus*, a small bipedal rodent with greatly elongated hindlimbs. In particular, the metatarsals of jerboa feet rapidly elongate during early postnatal development to approximately 2.5 times the relative proportion of mouse metatarsals[18]. The mouse distal metatarsal growth plate is intermediate in its growth rate and hypertrophic chondrocyte size compared to the mouse proximal tibia and radius (Fig. 2b and Supplementary Fig. 2). Although other aspects of the jerboa distal metatarsal growth plate are also altered, including the total cell number in each zone (Supplementary Fig. 3), the height of individual hypertrophic chondrocytes is increased by 58% compared to the metatarsal of the mouse, suggesting a significant contribution of hypertrophic chondrocyte volume to the increased rate of growth of this element (Fig. 2b, e, f). In contrast, the jerboa proximal tibia hypertrophic chondrocytes are only slightly larger than their counterparts in the mouse (Fig. 2b–d). Unlike the metatarsals, the metacarpals of the jerboa forelimb, as well as other bones of the forelimb, are similar in size and proportions to those of the mouse with hypertrophic chondrocytes of comparable size (Fig. 2b).

The hypertrophic chondrocytes of the jerboa proximal tibia show very similar growth properties to those of the mouse when examined by diffraction phase microscopy, including all three phases of volume enlargement (Supplementary Fig. 4). However, there is a striking difference between the metatarsal chondrocytes of the two species. Although mouse metatarsal hypertrophic chondrocytes are indeed intermediate in size between the proximal radius and proximal tibia, reaching a maximum volume of about 8,000 fl by completing phases 1 and 2 and truncating phase 3 (Fig. 2g), hypertrophic chondrocytes of the jerboa metatarsals increase almost 40-fold from their initial volume to approximately 23,000 fl, greater than the volume of tibia chondrocytes in either species (Fig. 2h). This is accomplished by following the

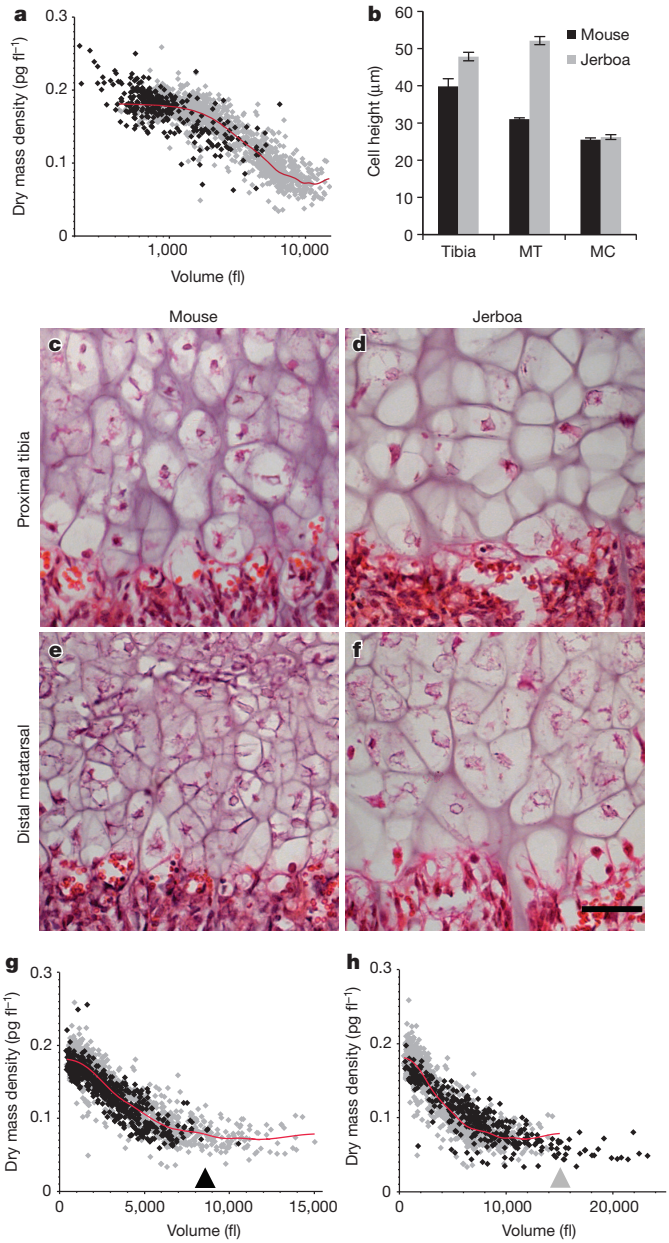

Figure 2 | Differences in cell size associated with different skeletal growth rates are attributed to modulating a common growth trajectory. **a**, Dissociated postnatal day 5 (P5) mouse proximal radius chondrocytes (black, $n = 292$ cells) compared to proximal tibia chondrocytes (grey in all panels, data from Fig. 1). The x axis is in log scale. **b**, Quantification of average maximum cell height ± s.e.m. for $n = 3$ animals of each species at P7 (>50 cells per growth plate). Two-tailed student's t-test shows significant differences in the tibia and metatarsal growth plates between the two species ($P < 10^{-5}$) but not in the metacarpals ($P = 0.978$). MC, metacarpal growth plate; MT, metatarsal growth plate. **c–f**, Histological comparison of mouse and jerboa proximal tibia and distal metatarsal hypertrophic zones at P7. Scale bar, 50 μm. **g**, Dissociated P5 mouse metatarsal chondrocytes (black, $n = 634$ cells) compared to mouse tibia chondrocytes. Black arrowhead approximates the end of the metatarsal distribution. **h**, Jerboa metatarsal chondrocytes (black, $n = 366$ cells) compared to mouse tibia chondrocytes. Grey arrowhead approximates the end of the mouse tibia distribution.

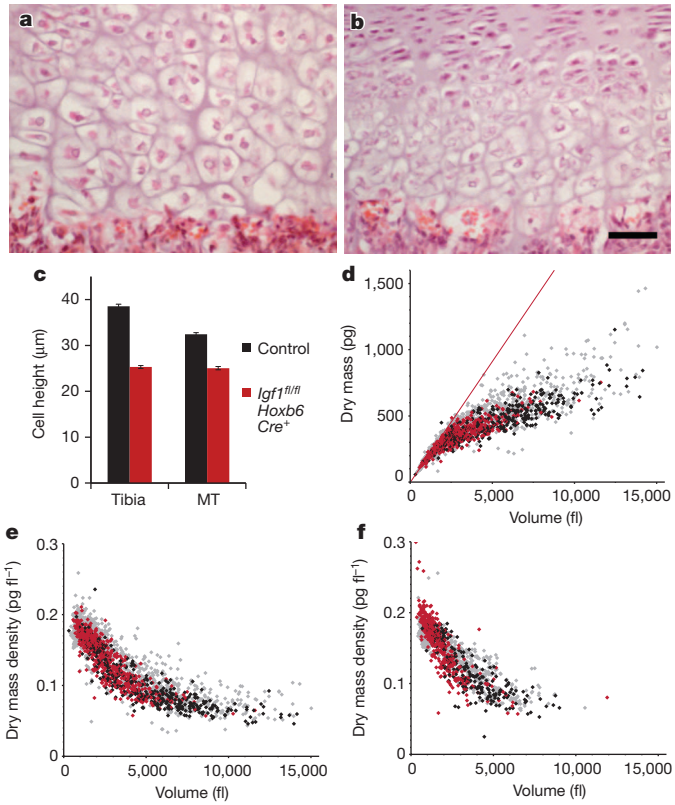

Figure 3 | *Igf1* is required for phase 3 of volume enlargement by dry mass production at low dry mass density. **a**, **b**, Histology of postnatal day 7 (P7) mouse proximal tibia hypertrophic zone of control (**a**, $Igf1^{fl/+}$; *Hoxb6-Cre*$^{+}$) and *Igf1* conditional mutant animals (**b**, $Igf1^{fl/fl}$; *Hoxb6-Cre*$^{+}$). Scale bar, 50 μm. **c**, Bar plot demonstrating an average maximum cell height reduction of 34% in *Igf1* conditional mutant tibia and 23% in metatarsal chondrocytes compared to control littermates. Error bars indicate ± s.e.m. for $n = 3$ animals of each genotype (total = >80 cells per growth plate). **d**, Dry mass versus volume plot of dissociated P5 *Igf1* mutant proximal tibia hypertrophic chondrocytes. Red data points are *Igf1* mutant chondrocytes ($n = 569$ cells), black are littermate control chondrocytes ($n = 373$ cells) and grey represent the total wild-type data set for tibia (**d**, **e**) and metatarsal (**f**) (wild-type data from Figs 1 and 2). **e**, **f**, Dry mass density versus volume plots for *Igf1* mutant tibia chondrocytes ($n = 569$ cells) (**e**) and *Igf1* mutant metatarsal chondrocytes ($n = 412$ cells) (**f**).

same triphasic growth trajectory common to chondrocytes of other growth plates and then extending phase 3 to reach a maximal volume by continued proportionate increase in dry mass and fluid volume at low dry mass density.

Little is known about the molecular mechanisms that control chondrocyte enlargement, or the regulation of final cell size, as few of the mutants affecting skeletal development have been examined for size of individual hypertrophic chondrocytes. An intriguing exception is the null mutation of the gene encoding insulin-like growth factor 1 (*Igf1*)[19]. *Igf1* functions in a variety of target tissues to promote protein synthesis and cell growth[19,20] and is strongly expressed in both proliferating and pre-hypertrophic chondrocytes. *Igf1*-deficient mice are 35% smaller than controls but have the same number of hypertrophic chondrocytes, although each cell is 30% shorter in the direction of elongation, a finding we confirmed in mice where the floxed $Igf1^{tm1Dlr}$ allele[21] was conditionally deleted from the hindlimb using *Hoxb6-Cre* (ref. 22) (Fig. 3a–c). It is additionally intriguing to note that there is no distinction between the heights of chondrocytes in the proximal tibia and distal metatarsal of this mutant (Fig. 3c), indicating that *Igf1* may play an important role in the establishment of growth-plate-dependent cell size. Although this effect could be modulated by any member of the *Igf1* signalling pathway, evidence suggests a possible role for the receptor, *Igf1R*, which maintains higher levels of

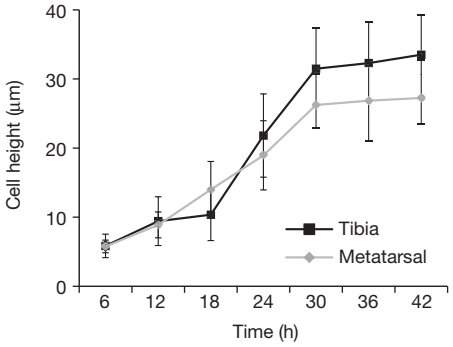

Figure 4 | Mouse proximal tibia and distal metatarsal hypertrophic chondrocytes rapidly increase in average cell height. Time course of the average and standard deviation of BrdU labelled cell height indicating the rate of chondrocyte size increase after the last mitotic cycle. $n > 25$ cells from three individuals for each time point and growth plate.

expression over time in growth plates that continue to elongate at faster rates in maturing mice[23].

We employed diffraction phase microscopy to determine which phase(s) of volume enlargement are affected by *Igf1*. *Igf1*-deficient hypertrophic chondrocytes undergo normal phase 1 and phase 2 of enlargement, reaching approximately 7,000 fl largely by cell swelling, but do not progress to phase 3 and thus fail to further double their volume by the continued production of dry mass at low density (Fig. 3d–f). Taken together, our results indicate that there are three distinct phases of chondrocyte hypertrophy, and it is regulation of the *Igf1*-dependent third phase that is responsible for much of the variation in skeletal elongation rate.

Finally, previous studies of the neonatal bat and mouse forelimb indicated that the entire hypertrophic zone of each growth plate turns over once in about 24 h regardless of the maximum volume attained by individual chondrocytes, the number of hypertrophic chondrocytes, or the rate of growth plate elongation[7]. This suggests that growth plates elongating at different rates adjust the rate of cell volume increase to fall within a 24-h lifespan constraint. To assess the pace of cellular maturation and enlargement, we marked proliferating mouse chondrocytes with 5-bromodeoxyuridine (BrdU) and followed the progression of the first labelled cells to emerge into the post-mitotic hypertrophic columns onward to the chondro-osseous junction (Supplementary Fig. 5). We find that the rate of cell height increase in the proximal tibia and distal metatarsal growth plates is extremely rapid, more than tripling the height of proximal tibia chondrocytes within approximately 12 h (Fig. 4). Once cells reach their average final height, with a steeper slope in the larger cells of the tibia, they remain at this terminal size in the hypertrophic growth columns for an additional 12 h before turnover at the chondro-osseous junction.

Through coordination of this multiphase process, cell swelling allows chondrocytes to enlarge extraordinarily rapidly while presumably lowering the energetic cost of growth, and volumes are subsequently amplified in the most rapidly elongating skeletal elements by the continued *Igf1*-dependent production of mass. This unique mechanism of volume enlargement suggests that chondrocyte hypertrophy will serve as a valuable model for cell volume homeostasis, in addition to our findings that provide insight into skeletal morphogenesis and evolution.

METHODS SUMMARY

The distal growth plate adjacent to the chondro-osseous junction was microdissected from P5 mouse and jerboa pups and dissociated for approximately 4 h in 2 mg ml^{-1} collagenase D at 37 °C. Cells were transferred to a 14-mm diameter glass-bottom dish for diffraction phase imaging. The specifications of the diffraction phase microscope are provided in the Supplementary Methods. The interference image, captured by charge coupled device (CCD), was used to compute a quantitative phase image in MATLAB. See Supplementary Methods for the

computation algorithm. The quantitative phase is converted to dry mass using the specific refractive increment value of $0.18\,ml\,g^{-1}$. For a subpopulation of cells, sphericity was determined using three-dimensional confocal morphometry and the refractive index contrast method (Supplementary Figs 12 and 13). As dissociated chondrocytes are spherical, we use the volume calculated from measured cell diameter for cells analysed by diffraction phase microscopy. Dry mass density was calculated by dividing the total cell dry mass by its volume. Dry mass density of a subset of cells was confirmed using regularized tomographic phase microscopy (Supplementary Fig. 14). See Supplementary Methods for details.

Full Methods and any associated references are available in the online version of the paper.

Received 18 March 2012; accepted 29 January 2013.
Published online 13 March 2013.

1. Wilsman, N. J., Farnum, C. E., Leiferman, E. M., Fry, M. & Barreto, C. Differential growth by growth plates as a function of multiple parameters of chondrocytic kinetics. *J. Orthop. Res.* **14,** 927–936 (1996).
2. Hunziker, E. B., Schenk, R. K. & Cruz-Orive, L. M. Quantitation of chondrocyte performance in growth-plate cartilage during longitudinal bone growth. *J. Bone Joint Surg. Am.* **69,** 162–173 (1987).
3. Hunziker, E. B. & Schenk, R. K. Physiological mechanisms adopted by chondrocytes in regulating longitudinal bone growth in rats. *J. Physiol. (Lond.)* **414,** 55–71 (1989).
4. Breur, G. J., VanEnkevort, B. A., Farnum, C. E. & Wilsman, N. J. Linear relationship between the volume of hypertrophic chondrocytes and the rate of longitudinal bone growth in growth plates. *J. Orthop. Res.* **9,** 348–359 (1991).
5. Kuhn, J. L., Delacey, J. H. & Leenellett, E. E. Relationship between bone growth rate and hypertrophic chondrocyte volume in New Zealand white rabbits of varying ages. *J. Orthop. Res.* **14,** 706–711 (1996).
6. Wilsman, N. J., Bernardini, E. S., Leiferman, E., Noonan, K. & Farnum, C. E. Age and pattern of the onset of differential growth among growth plates in rats. *J. Orthop. Res.* **26,** 1457–1465 (2008).
7. Farnum, C. E., Tinsley, M. & Hermanson, J. W. Forelimb versus hindlimb skeletal development in the big brown bat, *Eptesicus fuscus:* functional divergence is reflected in chondrocytic performance in autopodial growth plates. *Cells Tissues Organs* **187,** 35–47 (2008).
8. Buckwalter, J. A., Mower, D., Ungar, R., Schaeffer, J. & Ginsberg, B. Morphometric analysis of chondrocyte hypertrophy. *J. Bone Joint Surg. Am.* **68,** 243–255 (1986).
9. Farnum, C. E., Lee, R., O'Hara, K. & Urban, J. P. G. Volume increase in growth plate chondrocytes during hypertrophy: the contribution of organic osmolytes. *Bone* **30,** 574–581 (2002).
10. Bush, P. G., Parisinos, C. A. & Hall, A. C. The osmotic sensitivity of rat growth plate chondrocytes in situ; clarifying the mechanisms of hypertrophy. *J. Cell. Physiol.* **214,** 621–629 (2008).
11. Bush, P. G., Pritchard, M., Loqman, M. Y., Damron, T. A. & Hall, A. C. A key role for membrane transporter NKCC1 in mediating chondrocyte volume increase in the mammalian growth plate. *J. Bone Miner. Res.* **25,** 1594–1603 (2010).
12. Barer, R. Interference microscopy and mass determination. *Nature* **169,** 366–367 (1952).
13. Hoffmann, E. K., Lambert, I. H. & Pedersen, S. F. Physiology of cell volume regulation in vertebrates. *Physiol. Rev.* **89,** 193–277 (2009).
14. Hunziker, E. B. Mechanism of longitudinal bone growth and its regulation by growth plate chondrocytes. *Microsc. Res. Tech.* **28,** 505–519 (1994).
15. Kronenberg, H. M. Developmental regulation of the growth plate. *Nature* **423,** 332–336 (2003).
16. Popescu, G., Ikeda, T., Dasari, R. R. & Feld, M. S. Diffraction phase microscopy for quantifying cell structure and dynamics. *Opt. Lett.* **31,** 775–777 (2006).
17. Barer, R. Determination of dry mass, thickness, solid and water concentration in Living Cells. *Nature* **172,** 1097–1098 (1953).
18. Cooper, K. L. The lesser Egyptian jerboa, *Jaculus jaculus*: a unique rodent model for evolution and development. *Cold Spring Harb. Protocols* **2011,** pdb.emo066704 (2011).
19. Wang, J., Zhou, J. & Bondy, C. A. Igf1 promotes longitudinal bone growth by insulin-like actions augmenting chondrocyte hypertrophy. *FASEB J.* **13,** 1985–1990 (1999).
20. Oldham, S. & Hafen, E. Insulin/IGF and target of rapamycin signaling: a TOR de force in growth control. *Trends Cell Biol.* **13,** 79–85 (2003).
21. Yakar, S. Normal growth and development in the absence of hepatic insulin-like growth factor I. *Proc. Natl Acad. Sci. USA* **96,** 7324–7329 (1999).
22. Lowe, L. A., Yamada, S. & Kuehn, M. R. HoxB6-Cre transgenic mice express Cre recombinase in extra-embryonic mesoderm, in lateral plate and limb mesoderm and at the midbrain/hindbrain junction. *Genesis* **26,** 118–120 (2000).
23. Serrat, M. A., Lovejoy, C. O. & King, D. Age- and site-specific decline in insulin-like growth factor-I receptor expression is correlated with differential growth plate activity in the mouse hindlimb. *Anat. Rec. (Hoboken)* **290,** 375–381 (2007).

Supplementary Information is available in the online version of the paper.

Acknowledgements We would like to thank T. J. Mitchison, C. E. Farnum and members of the Developmental Bone Morphogenesis program project grant (National Institutes of Health (NIH)) for helpful discussions. We also thank the Nikon Imaging Center at Harvard Medical School for technical support, A. Luyten and R. Shivdasani for providing mouse megakaryocytes and P. Ramirez for jerboa care. This work was supported by NIH grants P01DK056246 to C.J.T.; R01GM026875 to M.W.K.; and by NIH grant P41RR02594, National Science Foundation (NSF) grant DBI0754339 and support from the Hamamatsu Corporation to R.R.D.

Author Contributions K.L.C. and S.O. conceived the project and carried out most of the experiments. Y.S. and R.R.D. carried out critical tomographic experiments validating the primary approaches taken. C.J.T. and M.W.K. supervised the project. K.L.C., S.O., M.W.K. and C.J.T. wrote the manuscript.

Author Information Reprints and permissions information is available at www.nature.com/reprints. The authors declare no competing financial interests. Readers are welcome to comment on the online version of the paper. Correspondence and requests for materials should be addressed to K.L.C. (kcooper@genetics.med.harvard.edu).

METHODS

Animals. CD-1 was chosen as the wild-type mouse strain for this study. *Igf1*^{tm1Dlr} conditional mice[21] and *Hoxb6-Cre* transgenic mice[22] were previously described. Jerboas were housed and reared as previously described[24]. All animal protocols were approved by the Harvard Medical Area Standing Committee on Animals.

Sectioning and histology. Dissected skeletal elements were fixed overnight at 4 °C in 4% paraformaldehyde and then carried through a graded series of ethanol dehydration washes before transition through xylenes and into paraffin wax. Sections were cut at 10–12-μm thickness and stained with haematoxylin and eosin. Average maximum cell heights were measured in the axis of linear growth through the lacunae surrounding the largest cells with a clear nuclear profile from digital images of the hypertrophic zone and averaged across at least 4 sections from at least 3 individuals. BrdU (100 mg kg^{-1}) or oxytetracycline hydrochloride (20 mg kg^{-1}) was injected into the peritoneum of P5 mice before harvest. BrdU was detected using a rat anti-BrdU antibody (AbD, Serotech) followed by goat anti-rat Alexa594 (Invitrogen) in paraffin sections. Oxytetracycline was detected by fluorescence in bisected skeletal elements.

Chondrocyte and megakaryocyte isolation. P5 animals were chosen for this study because the tibia and metatarsal growth plates are rapidly elongating in both species, but the metatarsal epiphysis (secondary ossification centre) has not yet formed. While the epiphysis of the metatarsal forms by P7 in the mouse, it appears later in the jerboa (Supplementary Fig. 3). As the hypertrophic chondrocytes reside in a small domain nearest the chondro-osseous junction, we enriched for these cells by using a razor blade to remove a majority of the cartilage containing resting and proliferative chondrocytes leaving the cells closest to the chondro-osseous junction and a small amount of the adjacent trabecular bone. Growth plates were bisected longitudinally and incubated for 45 min at 37 °C in 2 mg ml^{-1} collagenase D (Roche) in DMEM/F12 (Invitrogen, 290–330 mOsm) plus 10% fetal calf serum. After the initial incubation, the bone collar, trabecular bone and loosened connective tissues were manually removed with forceps, and the remaining cartilage fragments were transferred to a fresh dish of collagenase digestion media. Cells were incubated for an additional 2–3 h with occasional swirling until cells mostly dissociated from the surrounding matrix. Dissociated chondrocytes were transferred to 35-mm dishes with a 14-mm diameter, 1.5-thickness glass bottom (MatTek) and imaged immediately (see Supplementary Methods for details of imaging). The largest hypertrophic chondrocytes are a small population of the most mature cells, therefore we further enriched for this population in our data analysis by scanning for fields of view containing the largest cells in the dish and quantified all of the intact spherical neighbours.

There has been a longstanding discussion in the literature regarding the extracellular osmolarity of chondrocytes, primarily in the articular cartilage[9,10,25,26]. Much of this data are based on the theoretical ionic environment in association with charged glycosaminoglycans according to the Donnan-Gibbs equilibrium, although to our knowledge the extracellular osmolarity of growth plate cartilage has not been directly measured. While serum osmolarity is approximately 280 mOsm, the osmolarity in association with cartilage may be upwards of 400 mOsm. To address the possibility that the swelling we observe in chondrocytes at larger volumes may be the response to media of low osmolarity, we repeated the diffraction phase microscopy measurements in mouse proximal tibia growth plates dissociated in 424 mOsm DMEM/F12 raised with sucrose. Media osmolarity was measured using the Vapro Model 5600 (Wescor). We find the same three phases, including the phase of cell swelling, indicating this is an inherent property of growth plate chondrocytes and not the passive response to an abnormal osmotic environment (Supplementary Fig. 6). We presume that the 4 h from dissection to imaging is enough time for volume regulatory mechanisms to compensate for any response to osmotic stress that may have occurred. Indeed, 4D confocal imaging of *in situ* porcine articular chondrocytes after osmotic stress shows a mean recovery rate of 4.1% ± 1.8% per min with 96% volume recovery after about 12 min[27].

Fetal megakaryocytes were isolated from embryonic day 14.5 mouse livers according to previously published protocols[28,29] or generously donated by A. Luyten and R. Shivdasani. Cells were imaged by diffraction phase microscopy one day after harvest or at maturity after five days in culture.

24. Jordan, B., Vercammen, P. & Cooper, K. L. Husbandry and breeding of the lesser Egyptian jerboa, *Jaculus jaculus*. *Cold Spring Harb Protocols* **2011,** http://dx.doi.org/10.1101/pdb.prot066712 (2011).
25. Maroudas, A. & Evans, H. A study of ionic equilibria in cartilage. *Connect. Tissue Res.* **1,** 69–77 (1972).
26. Urban, J. P. G., Hall, A. C. & Gehl, K. A. Regulation of matrix synthesis rates by the ionic and osmotic environment of articular chondrocytes. *J. Cell. Physiol.* **154,** 262–270 (1993).
27. Errington, R. J., Fricker, M. D., Wood, J. L., Hall, A. C. & White, N. S. Four-dimensional imaging of living chondrocytes in cartilage using confocal microscopy: a pragmatic approach. *Am. J. Physiol.* **272,** C1040–C1051 (1997).
28. Lecine, P., Blank, V. & Shivdasani, R. Characterization of the hematopoietic transcription factor NF-E2 in primary murine megakaryocytes. *J. Biol. Chem.* **273,** 7572–7578 (1998).
29. Shivdasani, R. A. & Schulze, H. Culture, expansion, and differentiation of murine megakaryocytes. *Current Protocols Immunol.* http://dx.doi.org/10.1002/0471142735.im22f06s67 (2005).